Initial conditions of radiative shock experiments[a)]

C. C. Kuranz,[1,b)] R. P. Drake,[1] C. M. Krauland,[1] D. C. Marion,[1] M. J. Grosskopf,[1] E. Rutter,[1] B. Torralva,[1] J. P. Holloway,[1] D. Bingham,[2] J. Goh,[2] T. R. Boehly,[3] and A. T. Sorce[3]
[1]*Department of Atmospheric, Oceanic and Space Science, University of Michigan, Center for Radiative Shock Hydrodynamics, 2455 Hayward Dr., Ann Arbor, Michigan 48109, USA*
[2]*Department of Statistics and Actuarial Science, Simon Fraser University, Burnaby, BC, Canada V5A 1S6*
[3]*Laboratory for Laser Energetics, University of Rochester, New York 14623, USA*

(Received 14 December 2012; accepted 26 March 2013; published online 31 May 2013)

We performed experiments at the Omega Laser Facility to characterize the initial, laser-driven state of a radiative shock experiment. These experiments aimed to measure the shock breakout time from a thin, laser-irradiated Be disk. The data are then used to inform a range of valid model parameters, such as electron flux limiter and polytropic γ, used when simulating radiative shock experiments using radiation hydrodynamics codes. The characterization experiment and the radiative shock experiment use a laser irradiance of $\sim 7 \times 10^{14}$ W cm^{-2} to launch a shock in the Be disk. A velocity interferometer and a streaked optical pyrometer were used to infer the amount of time for the shock to move through the Be disk. The experimental results were compared with simulation results from the Hyades code, which can be used to model the initial conditions of a radiative shock system using the CRASH code. © *2013 AIP Publishing LLC*. [http://dx.doi.org/10.1063/1.4805021]

I. INTRODUCTION

Radiative shocks occur when the energy flux due to thermal radiative loss from a system approaches the energy flux from the shocked material. When this occurs, the radiation affects the hydrodynamic structure of the system. These types of shocks are found in some accretion phenomena, supernovae and stellar shocks.[1–6] Further discussion of astrophysical connections is in the paper by Drake.[7] There are different types of radiative shocks depending on the opacity of the upstream (unshocked) and downstream (shocked) materials, and in some cases Mach number.[8,9] The system we are studying has an optically thick downstream region and a upstream region from which radiation readily escapes. The escaping radiation heats the region ahead of the shock, which is referred to as the radiative precursor region. The radiative losses cause the region behind the shock to cool rapidly. The drop in temperature causes the volume of the post-shock region to decrease creating a "collapsed layer." This leads to a compression of the shocked material being much higher than 4, which is the maximum compression due to hydrodynamic shock.

Radiative shocks have been created and studied at high-energy-density facilities around the world. Several of these experiments use an energy source, which can be a high-energy laser, to launch a piston into a low-density gas or foam.[7,10–18] The result is generally a very fast moving shock with large radiative fluxes. Other experiments create a radiative blast wave by local energy deposition in a low-density material, which can lead to secondary shocks or unstable structures.[19–24]

For more than a decade, we have been studying the piston-driven radiative shock system.[7,13,17,25–28] These experiments use the Omega Laser Facility[29] to deposit kilojoules of energy into a sub-millimeter spot on a thin Be disk. This disk is accelerated into a polyimide ($C_{22}H_{10}N_2O_5$) tube filled with Xe gas at 1.1 atm. This creates a fast moving (greater than 100 km/s) shock that has significant radiative loses. The target structure also includes gold and acrylic shielding for diagnostic purposes. An x-ray radiograph of this experimental system is shown in the left panel of Figure 1. The dark regions in this image are typically shocked Xe, in which plasma is flowing to the right and the laser was incident from the left. A fiducial grid on the upper portion of the image is used for calibration. The shock position is about 2.2 mm from the Be disk and the shocked Xe layer is about 120 μm thick, which indicates a compression ratio of over 18. The shocked Xe layer may be thinner than observed due to tilt, which would result in higher compression ratios.[27]

Due to their complexity, radiative shock systems are difficult to model. The Center for Radiative Hydrodynamics (CRASH) at University of Michigan is developing a 3D radiation hydrodynamics code in an effort to simulate systems of this type.[30,31] The CRASH code is an Eulerian, flux-limited multigroup diffusion, radiation hydrodynamics code. In initial work with CRASH, the laser-energy deposition has been modeled using the 2D Hyades code.[32] A simulated radiograph from CRASH simulation output of a radiative shock experiment is shown in the right panel of Figure 1. The parameters of the simulation were similar to those of the experiment.

There are numerous detailed differences between the experimental and simulated radiographs. Some of these reflect the fact that the simulation is 2D while there is clearly some 3D structure in the experiment. But even allowing for this, the morphology of the simulated shock was clearly different from that in the experiment. Examination of the simulated parameters showed that this reflected a complex interplay of radial and axial flows. This led us to conclude that understanding the behavior of the shock in the Be was essential to assure that the simulation was starting with the correct energy and momentum content. This in turn led to the experiments

[a)]Paper BI3 5, Bull. Am. Phys. Soc. **57**, 26 (2012).
[b)]Invited speaker. Electronic mail: ckuranz@umich.edu

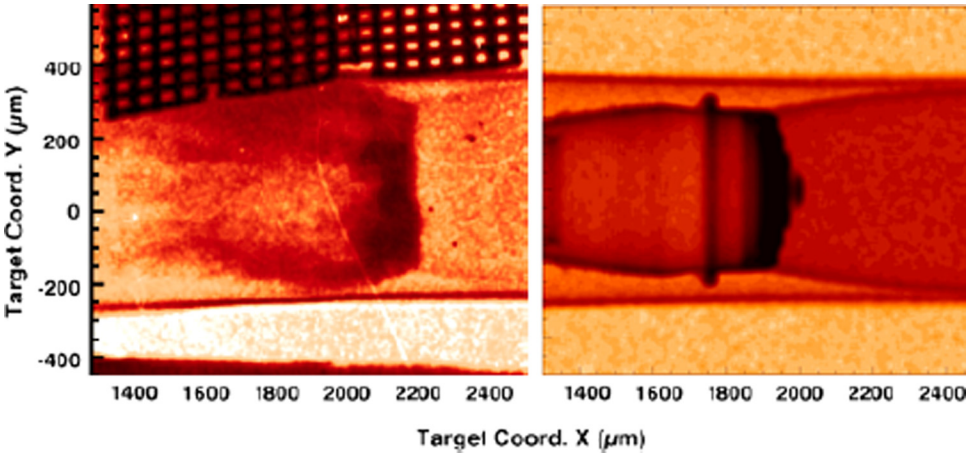

FIG. 1. (Left) An x-ray radiograph of a radiative shock. The shock is moving to the right and was imaged at 14 ns after the initialization of the laser pulse. The dark regions in this radiograph indicate dense material. The Be disk is behind the compressed Xe layer, but is not visible due to its lower relative opacity. This image is adapted from Doss *et al.* 2010.[27] (right) A simulated radiograph from such a CRASH simulation results showing a radiative shock at t = 14 ns.

discussed here. The measurement used to study the initial conditions was the time it takes for the shock to move through or "breakout" of the Be disk. This is often referred to as the shock breakout time. The shock breakout time can aid in the determination of model parameters, such as the electron flux limiter and polytropic γ of Be. In this paper, experiments performed to understand the laser-driven state that initializes the radiative shock experiment are detailed.

Previously, many experiments have been performed that study the conditions before and when a shock wave breaks out of a material. The purposes of these experiments include measuring the ablation pressure deposited in the material,[33] measuring the refractive index of a material,[34] estimating preheat in a system,[35,36] and studying the equation of state (EOS) of the material.[37] The results from these experiments are used to inform studies of inertial confinement fusion,[38] planetary interiors,[39] and hydrodynamics instabilities.[35,40] Shock breakout experiments typically use a velocity interferometer and optical pyrometer as diagnostics.

While each radiative shock experiment is performed under nominally the same conditions, there are variations in some experimental parameters, for example, laser energy, Be disk thickness, and Xe gas pressure. When modeling the experiment, some parameters are used that cannot be directly measured in the experiment, such as, the electron flux limiter and the equation of state of the material, represented here by a polytropic index (ratio of specific heats) γ. Simulations with the Hyades and CRASH codes were used to help understand the effects of the variations in experimental parameters and a valid range for model parameters.

In this paper, we describe shock breakout experiments that support the understanding of the experimental initial conditions and the modeling parameters used in simulating the radiative shock experiment. The experimental data are compared to 2D Hyades simulations in which the polytropic γ of Be, laser energy, electron flux limiter, Be thickness, and polyimide wall opacity are varied.

II. EXPERIMENTAL SETUP AND DIAGNOSTICS

To characterize the initial state of the radiative shock experiment, we performed 12 experiments to measure the shock breakout from a Be disk over three experimental days. The majority of the Be disk thicknesses ranged from 19 to 21 μm ± 0.5 μm where the average disk thickness was 19.9 μm with a standard deviation of 0.6 μm. Two experiments were performed with a 10 μm ± 0.5 μm disk. Each Be disk was irradiated with ten Omega laser beams that were smoothed with a Distributed Phase Plate (DPP), which creates a spatial profile of a super-Gaussian with an exponent of 4.5 and a laser spot size of about 820 μm FWHM. The laser beams are further smoothed by the temporal beam-smoothing technique Smoothing by Spectral Dispersion (SSD) to produce moving speckles in the beam spot about 5 μm in size. The requested total laser energy was 3.8 kJ. For the 12 experiments performed, the on-target total laser energy averaged 3.841 kJ ± 0.001 kJ. The range of laser energy for these experiments was 3.403 kJ–3.946 kJ with a standard deviation of 0.152 kJ. The laser pulse was a 1 ns square pulse with about 100 ps of rise and fall time. The nominal on-target laser irradiance was about 7×10^{14} W/cm^2.

The ablation pressure produced by the laser beams launches a shock into the Be disk and the emergence of that shock from the rear surface is recorded on multiple experimental diagnostics. These diagnostics are calibrated and the amount of time it takes for the shock to move through the Be disk is inferred. Three instruments were used on each experiment to make these measurements and in the majority of experiments all three collected data.

Two of the instruments were a Velocity Interferometer System for Any Reflector (VISAR)[41] set to different sensitivities. A VISAR uses a laser with a wavelength of 532 nm to probe a surface and detect the rate of change in the optical path to a surface. This can lead to a measurement of a velocity profile of a surface from which one can infer average pressures. For the experiment reported here, the probe laser is reflected off of the rear (non laser-irradiated side) of the Be disk as shown in Figure 2. Since the Be disk is opaque to the probe laser light, only movement on the rear surface, such as the shock exiting the rear surface of the disk, is recorded. This is referred as shock breakout and the time it takes for this to occur is referred to as the shock breakout time. This will yield an average shock velocity in the Be disk and an average pressure by the relation

$$P_2 = \frac{2}{(\gamma+1)}\rho_1 u_s^2\left[1 - \frac{(\gamma-1)P_1}{2\rho_1 u_s^2}\right], \quad (1)$$

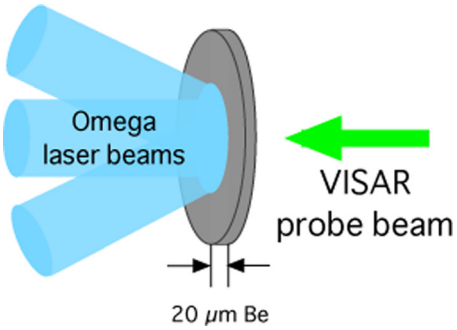

FIG. 2. A schematic of the target. A nominally 20 μm Be disk is irradiated with several laser beams. The diagnostics (2 VISARs and SOP) view the rear surface of the target and measure the shock breakout time.

where P_2 and P_1 are the upstream and dowstream pressures, respectively, γ is the post-shock polytropic index, and u_s is the shock velocity. For a strong shock, $P_2 \gg P_1$ and $2/(\gamma+1)$ is of order 1 so Eq. (1) can be approximated as $P_2 \sim \rho u_s^2$.

The third diagnostic used to measure the shock breakout time was a Streaked Optical Pyrometer (SOP).[42] A SOP is a passive detector that records thermal emission on a streak camera which results in a 2D image showing the surface emission in space and time. SOP views the rear surface of the target and as the hot shock emerges from the rear of the Be disk its emission will be recorded with the SOP, from which the breakout time can be inferred.

Examples of the typical VISAR and SOP data from this experiment are shown in Figure 3. The SOP data are shown in the left panel with time increasing to the right. There is no detectable emission from the rear surface of the target until the shock emerges from the rear surface of the disk. The thin bright line on the left of this image occurs as the laser pulse is initiated although for unknown reasons. It should be noted that the SOP (and VISAR) data show curvature in the breakout feature. This is due to the profile of the laser spot, which results in a curved shock as the Be disk is larger than the laser spot. For the radiative shock experiment, the shock tube is 575 μm in diameter and the shock breakout feature is relatively planar over that region.

The VISAR data are shown in the right panel in Figure 3 with time increasing to the right. In this case, the probe beam is reflected off of the rear surface of the Be disk, which produces the bright signal on the left. The thin, bright line in the image is the shock breaking out of the Be disk. Prior to shock breakout, there is an area on the image with no signal. This occurs after the initial laser pulse has begun and the VISAR probe beam is absorbed, which often occurs at high laser irradiances,[43] until the shock breaks out of the disk and the shock itself is reflective.

Typically a VISAR uses a probe beam to detect the rate of change in the derivative of the optical path to the surface. In this experiment, some shots were performed in this mode and the motion of the surface before shock breakout was found to be very small and difficult to detect. For the majority of the experiments, the diagnostic was used in a mode where only the shock breakout was detected and not the motion on the surface.

Both of these VISAR and SOP measurements can be calibrated in time using the timing fiducials, which are created with an optical laser, seen at the bottom of both of the images shown in Figure 3. The shock breakout time was measured to the 50% rise of the feature indicating breakout. To discern individuals experiments, the thickness of each disk has been offset 0.2 μm. The 3 data points for each disk are from the 2 VISARs and the SOP instruments. In some cases, 1 or 2 of the diagnostics did not produce usable data. The vertical error bars on each point are due to the error in each diagnostic measurement, which is due to the sensitivity of the measurement. The VISARs (set to different sensitivities) were the most sensitive and had errors of $\pm$10 ps and $\pm$20 ps while the SOP had a larger error of $\pm$30 ps. The error in the disk thickness is $\pm$0.5 μm.

There exists a larger systematic error in the time calibration due to the timing of the fiducial laser relative to the laser pulse used to irradiate the disk. The timing of these 2 lasers is known to $\pm$50 ps. This timing should be consistent on a single experimental day, but the data shown in Figure 4 were

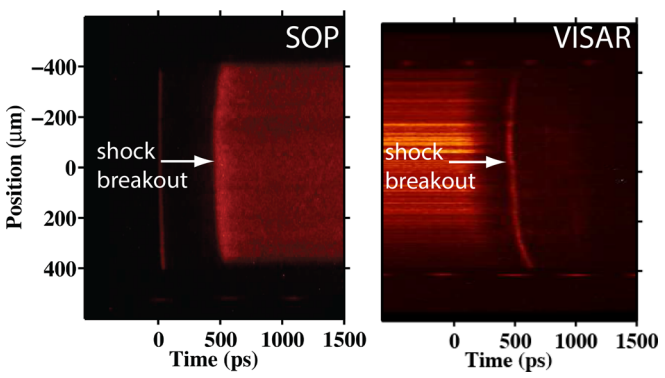

FIG. 3. Typical data from experiments performed with a nominally 20 μm thick Be disk from the SOP (left panel) and VISAR (right panel). Both diagnostics view an 800 μm high region on the rear surface of the Be disk and record when the shock breaks out of the disk. The fiducials on the bottom of each image are spaced 548 ps apart.

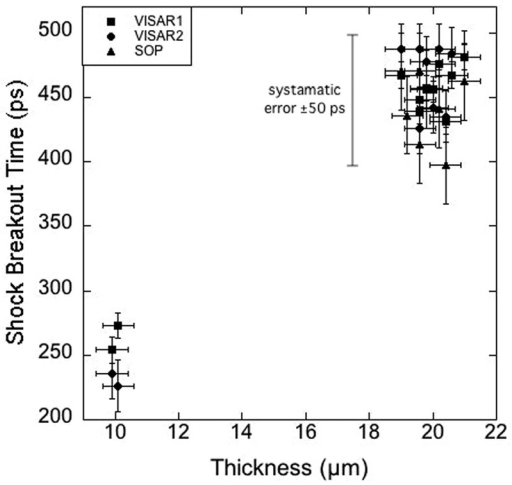

FIG. 4. Shock breakout time for Be disks of 19, 20, and 21 μm. Data points are offset in thickness to discern between individual experiments. The error bars on individual points indicate the uncertainty due to that diagnostic and the larger error bar on the right represents the systematic error in the experiment due to the uncertainty in the timing of the laser pulse irradiating the Be disk and the laser pulse that creates the fiducial shown at the bottom of the experimental images in Figure 3.

taken over 3 experimental days so the maximum credible offset for the data set is ±50 ps. The systematic timing error is the largest error for the data and encompasses the entire timing range observed, which was 397–487 ps. This is indicated by a ±50 ps error bar on the plot. Under the experimental conditions described above, the average shock breakout time for the nominally 20 μm disk was 457 ps.

III. SIMULATIONS

Due to the difficulty in creating and diagnosing high-energy-density physics experiments, experimental data are often limited. Computer models can assist in the planning and understanding of experiments. However, it can be difficult to ascertain the value of a model parameter that cannot be directly measured in the experiment, such as electron flux limiter and polytropic γ of Be. Simulation results can also be used to determine the effect of experimental parameters that vary between experiments, such as laser energy and Be disk thickness. Simulations to model the laser-driven state of the Be disk were performed with the 2D Hyades code.

The Hyades code is a one- and two-dimensional, Lagrangian code with a multigroup, flux-limited diffusion radiative transport model. Hyades uses equations that describe a three-temperature, single fluid. The pressure in the momentum and energy equations represents the summed contributions from electrons, ions, and radiation. There is an energy equation for ions, for electrons, and for each radiation group. Electron heat transport is modeled by single group, flux-limited diffusion. Multi-group radiation allows the user to assign energy ranges to many different photon groups, for each of which the opacity is calculated using an average atom model. Hyades also includes a laser-energy deposition model that here modeled the incoming laser beams in two dimensions. Results from Hyades simulations can be used to initiate CRASH simulations.

A total of 104 simulations were performed using the 2D Hyades code varying the Be polytropic γ, laser energy, electron flux limiter, Be thickness, and the opacity of the polyimide wall. The majority of these parameters were chosen because a previous sensitivity study, performed with 1D Hyades, indicated that the shock position was most sensitive to these parameters. The exception is the wall opacity, which was studied because it could not be modeled in 1D simulations. These simulations modeled the radiative shock experiment, which includes Xe gas, gold, and acrylic shielding material. However, for purposes of the experiments detailed in this paper, only the behavior of the shock in the Be disk is of interest. It should not be affected by the other materials in the model.

The laser energy refers to the total laser energy on target and the Be thickness is the overall thickness of the Be disk. The electron flux limiter is used to reduce the amount of energy transported via electron thermal conduction in laser-irradiated materials.[44,45] In these simulations, a gamma-law EOS was used to model the Be as an ideal gas. In this case, $P = (\gamma - 1)\rho\epsilon$, where P is the pressure, ρ is the mass density, ϵ is the specific internal energy, and γ is the polytropic index. For a fully ionized gas, γ is equal to 5/3; it is smaller for a partially ionized material, such as the Be here.[46] The wall opacity refers to the opacity of the polyimide tube wall. The opacity is defined as $\rho\mu$, where ρ is the mass density and μ is the mass absorption coefficient and is specific to material and wavelength of light being attenuated by the material. In the simulation, the opacity of the polyimide wall was varied using a scale factor f and the opacity was modeled as $f\rho\mu$. The experiment detailed in the present paper does not include a polyimide tube, only the Be disk. However, the radiative shock experiment described in earlier papers[13,17,25] includes a polyimide shock tube, which hold the Xe or, in some cases, Ar gas. It has been observed that the polyimide tube absorbs some of the radiation emitted upstream of the shock[26] and the opacity of the tube could affect the amount of radiation emitted from the target.

The range of each of the five parameters varied is shown in Table I. The parameter values used for each of the 104 Hyades simulations were constructed using a 64 point orthogonal latin hypercube over the 5 dimensional input space, with a space filling criterion. Forty additional sample points were then selected in 4 sequential groups of 10 points each to fill in holes in input space. Many studies use latin hypercubes to sample a large parameter space while minimizing computing cost.

A contour plot of the density from the results of a Hyades simulation is shown in Figure 5. The shock is moving to the right and is about 700 μm from the laser-irradiated surface of the Be. Also, the laser-ablated plasma is moving to the left. Additional simulation results from the full set of simulations are shown in Figures 6–9. These 4 plots show the shock breakout time (the amount of time it takes the shock to reach the rear of the Be disk for that particular simulation) versus one of the five parameters varied. The uncertainty in the shock breakout time is approximately the size of the marker. The black horizontal line in Figures 6–9 indicates the average experimental shock breakout time and the shaded area is the full range of experimental shock breakout times for the 19, 20, and 21 μm Be disks.

IV. DISCUSSION

When comparing the results of the simulations to experimental data, one must consider the definition of t = 0. For the simulation, t = 0 is the defined at the initiation of the laser pulse. For the experiment, t = 0 is 2% of the maximum on the rising edge of the laser pulse. The difference only a few picoseconds and will be taken as part of the uncertainty in the measurement so that the simulation and experimental shock breakout times will be compared directly.

TABLE I. Input range of the parameters varied in the 104 2D Hyades simulations.

Parameter	Input range
Be γ	1.40–1.75
Flux limiter	0.05–0.075
Be thickness (μm)	18–22
Laser energy (kJ)	3.6–4.0
Wall opacity scale factor	0.7–1.4

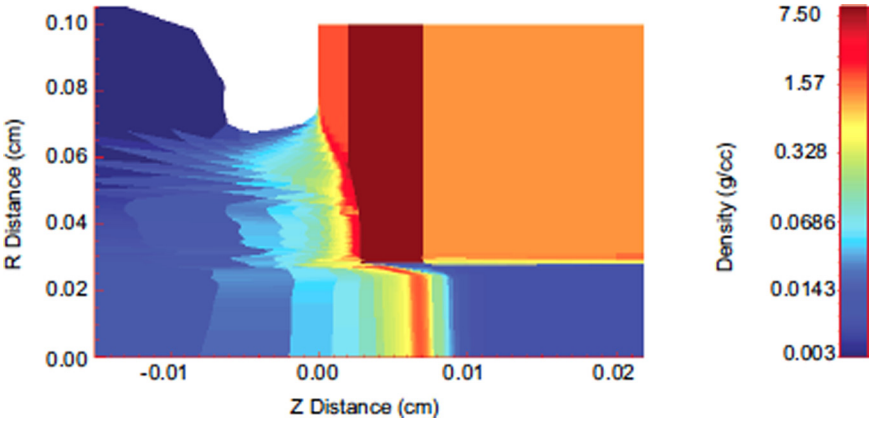

FIG. 5. Simulation output from a 2D Hyades simulation of a radiative shock experiment at 4.5 ns. This image shows the density along the shock tube and in the radial direction. The shock is moving to the right and the laser is incident from the left.

Figure 6 shows the shock breakout time versus the polytropic γ of Be. The steep negative slope in the plot indicates that Be γ has a strong negative correlation to the shock breakout time. As Be γ increases, the shock breakout time decreases which also corresponds to the shock moving faster. Comparing to the average experimental breakout time, the best value range for Be γ is about 1.4–1.55. This is less than the value for fully ionized Be, and is consistent with the SESAME tables. The result is sensible since the Be temperature is 50 eV here while the fourth ionization energy of Be is >200 eV. However, the strong dependence on Be γ came as a surprise to us. While Eq. (1) does imply that a smaller value of γ corresponds to a smaller shock velocity at constant ablation pressure, the difference in shock velocity for the range of γ used would be 7%, while instead the observed difference exceeds 25%. There would appear to be a nonlinear connection of post-shock density and ablation pressure in the simulations, but we do not understand its origins.

Figure 7 shows the shock breakout time versus electron flux limiter. The input range for electron flux limiter was 0.05 to 0.075. There is a slight negative slope on this plot, which is expected since more energy is transported via electron heat conduction as the electron flux limiter increases corresponding to a higher ablation pressure, faster shock velocity, and shorter shock breakout time. However, the simulated shock breakout time falls into the experimental range for all flux limiter values. Typical values for the electron flux limiter from the literature are 0.05 and 0.06.[44,45]

Figure 8 shows the shock breakout time versus Be disk thickness. This plot shows a positive slope meaning that the thicker the disk the longer it takes for the shock to pass through it. This conclusion is to be expected, but it should be noted that the simulation output covers the experimental range of data even though the experimental range of Be thickness is slightly less than that sampled in the models. The experimental average tends toward thicker Be disks even though the average disk thickness was 19.9 μm.

Figure 9 show the shock breakout time versus total laser energy. It is worth noting that the experimental laser range is slightly larger than the range sampled in the simulations. This is due to 1 experiment that had a low on-target energy (3.4 kJ). This plot indicates that any correlation between laser energy and shock breakout time is much smaller than the correlation with other variables in the run set. This is similar to the finding of the experiment, which indicates that within the experimental error the laser energy does not have an effect on

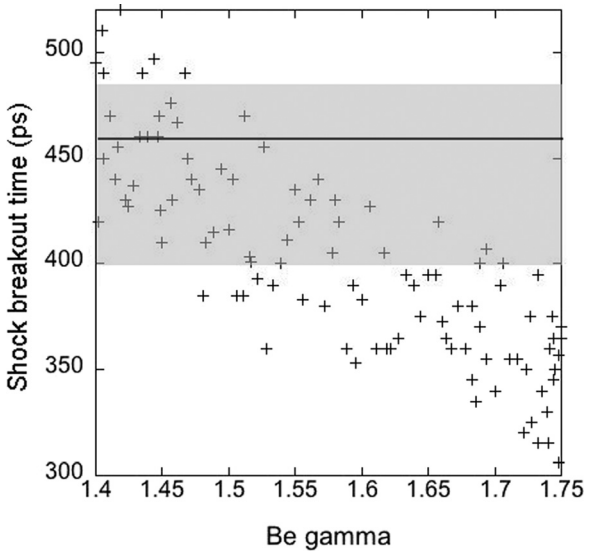

FIG. 6. A plot of shock breakout time versus the Be γ for the 104 2D Hyades simulations with the experimental average at 450 ps shock by the black line and the experimental range shown by the gray region.

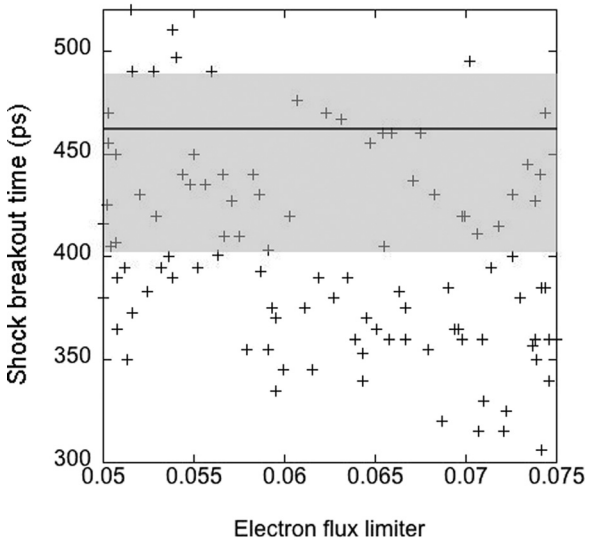

FIG. 7. A plot of shock breakout time versus the electron flux limiter for the 104 2D Hyades simulations with the experimental average at 450 ps shock by the black line and the experimental range shown by the gray region.

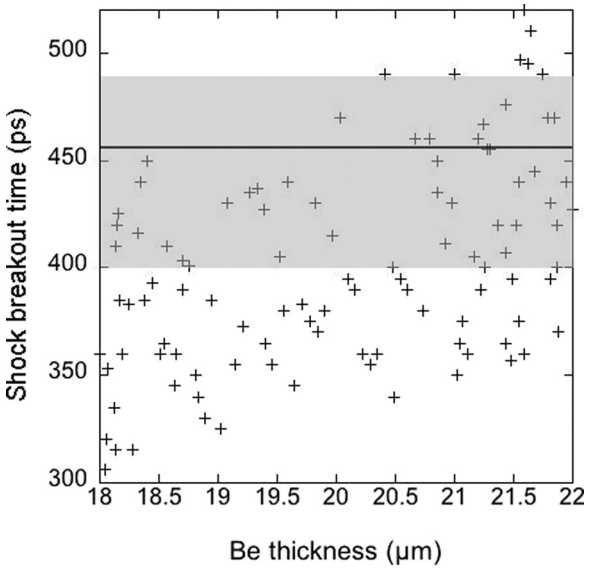

FIG. 8. A plot of shock breakout time versus the Be thickness for the 104 2D Hyades simulations with the experimental average at 450 ps shock by the black line and the experimental range shown by the gray region.

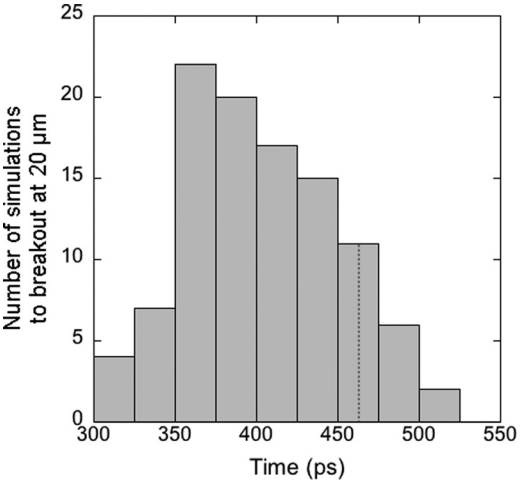

FIG. 10. A histogram of shock breakout times from 2D Hyades simulation results with the experimental average indicated by the black dashed line. The majority of the simulations have a shock breakout time earlier than the experimental average.

the shock breakout time. Note that this does not indicate that the laser energy has no effect on shock velocity for the radiative shock experiment described in the Introduction of this paper. It is possible that at such early times (about 450 ps) the effect of laser energy on shock location is small but that it becomes larger at later times when the radiative shock is observed (about 13 ns).

The plot of the shock breakout time versus wall opacity is similar to Figure 9 and shows no correlation to the shock breakout time. The wall opacity should have no effect on shock breakout time but, again, could have an effect on the radiative shock experiment.

Figure 10 shows a histogram of the frequency of the shock break times with bins of 25 ps. The average experimental shock breakout time is indicated by the dashed line at 457 ps. The majority of the simulations (89 of the 104) have shock breakout times prior to the experimental average. This is more clearly seen in Figure 11. This is a plot of shock position versus time with output from all the of 104 Hyades simulations. All of the simulation output falls into the gray region with the black lines being the bounding edges of the simulation output. The experimental data are also plotted with the shock position being the thickness of the Be disk. From this plot, it can be seen that the data overlap with the upper part of the simulations with some simulations having no overlap with the experiment and for the majority of the simulations the shock is moving faster in the simulations.

The discrepancy between the simulation and the experiment could be related to multiple factors. It is possible that the input range that was sampled is unphysical, which can inform the input range for future simulations. For example,

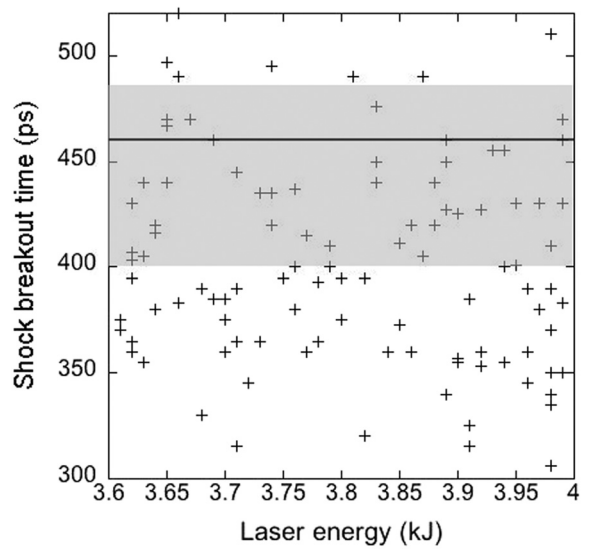

FIG. 9. A plot of shock breakout time versus the laser energy for the 104 2D Hyades simulations with the experimental average at 450 ps shock by the black line and the experimental range shown by the gray region.

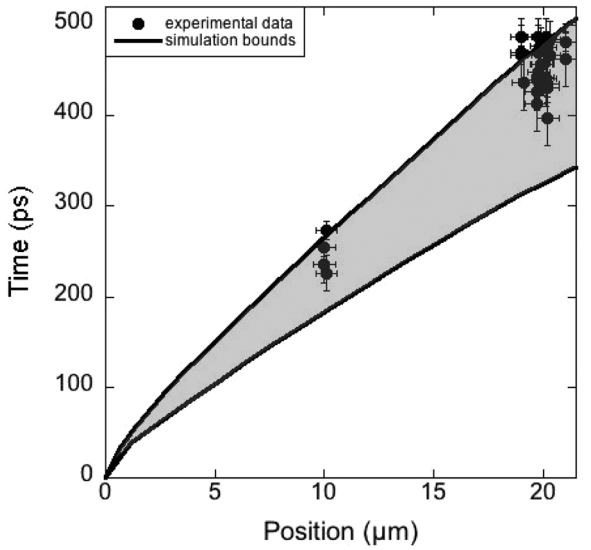

FIG. 11. Shock position versus time for the experiment and all simulation results. All simulation results fall between the 2 black lines in the shaded gray region.

due the strong dependance between the shock breakout time and Be γ, future simulations will likely have a narrower input range for this parameter, possibly 1.4 to 1.6. Also, the range for electron flux limiter could have been smaller and possibly included lower values. Values used frequently in similar models are 0.05 and 0.06 while we sampled the range 0.05–0.075 and allow the available simulations and observations to constrain the values for the electron flux limiter. Using smaller values for electron flux limiter would cause the shock velocity to decrease and therefore shock breakout time would increase.

It is possible that laser-plasma instabilities are present in the experiment and reduce the amount of laser energy deposited in the Be disk resulting in a lower ablation pressure and therefore a longer shock breakout time. However, at this laser irradiance, it is unlikely that this will account for much energy being lost. Future experiments are planned to make a measurement of the backscattered laser light to indicate the effects of laser-plasma instabilities.

The best values of the parameters, Be γ, electron flux limiter, and the polyimide opacity scale factor, can be determined by solving a type of inverse inverse problem. More specifically, a Bayesian hierarchical model[47] is used to combine observations and simulations to provide estimates of these three parameters. The basis for this approach is found in Kennedy and O'Hagan[48] and Higdon *et al.*[49] and is described briefly below. As an aside, we note that statistics literature refers to this type of inverse problem as *model calibration* and the parameters of interest (Be γ, electron flux limiter, and polyimide opacity scale factor) as *calibration parameters*. We will adopt these terms in our discussion for consistency.

The approach that we use writes the observations as the sum of the simulator output, a discrepancy term and observation error. That is,

$$y(\mathbf{x}) = \eta(\mathbf{x}, \theta) + \delta(\mathbf{x}) + \epsilon, \tag{2}$$

where $y(\mathbf{x})$ denotes an observed quantity of interest at input setting $\mathbf{x}$ (i.e., the variables that we can adjust and/or measure in the experiment), θ is the vector of calibration parameters to be estimated, $\eta(\mathbf{x}, \theta)$ is the simulator output at input settings $(\mathbf{x}, \theta)$, $\delta(\mathbf{x})$ is the discrepancy that accounts for systematic differences between the code output and the system mean, and ϵ is observation error. Note that a CRASH code run takes in inputs $\boldsymbol{t}$ in place of the true calibration parameters θ and many different combinations of Be γ, electron flux limiter, and the polyimide opacity scale factor are explored in the simulations. However, the value of the calibration parameter in the field, θ, is unknown and has to be estimated as part of fitting the Bayesian hierarchical model.

To set up the Bayesian hierarchical model, Gaussian process models[50] are used to estimate the response surfaces η and δ and the errors are assumed to be independent and identically distributed normal random variables. This in turn implies a multivariate normal likelihood for the vector of experimental observations and simulations. Next prior distributions are chosen for the parameters of the statistical model (denote these as $\boldsymbol{\rho}$) and the calibration parameters θ. For the calibration parameters, the prior distributions are generally constant over the assumed range (i.e., uniform distributions) to represent our prior belief of their values. Bayes' theorem is used to combine data (observations and simulations) with the prior distribution for the parameters to obtain the posterior distribution of the parameters of interest:

$$p(\theta, \boldsymbol{\rho}|data) \propto p(\text{data}|\theta, \boldsymbol{\rho}) p(\theta, \boldsymbol{\rho}),$$

where we use p to generically denote a distribution and $p(\theta, \boldsymbol{\rho}|data)$ is called the posterior distribution of parameters. The posterior distribution of calibration parameters, $p(\theta|data)$, is found by integrating out the statistical model parameter from the posterior distribution above.

A sample for the posterior distribution of the parameters is obtained using Markov chain Monte Carlo (MCMC).[49] Using this distribution, we can determine the mode, median, or the mean of the posterior distribution and use this as the single nominal value for the calibration parameters. Also, we can study the posterior distribution of calibration parameter values to understand the uncertainty in the simulation due to uncertainty in the calibration parameters. Figure 12 shows the joint posterior distribution of the electron flux limiter and Be γ. Note that there is a correlation between the best flux limiter values and the Be γ, with smaller values of γ correlated with higher values of the electron flux limiter. We have also examined the joint posterior distributions of the other parameters studied, but found the strongest correlation to be between the Be γ and the electron flux limiter.

The Hyades code is able to model the laser beam irradiating the Be disk in two or three dimensions. However, the number of rays needed and the run times required for modeling in three dimensions are quite large, and so the present set of runs was done modeling the rays in two dimensions. In the experiment, the incoming beams are focused on the center of the disk, but offset by 2 angles. Since the simulation does not model one of these angles, one would expect that the amount of laser energy deposited in the target would be higher than in the experiment. This would result in a higher ablation pressure, faster shock, and shorter shock breakout time, which is what seen in the simulation results.

One can also estimate an average pressure of the system by using an average shock velocity (the disk thickness divided by the shock breakout time) using Eq. (1). The measured quantity is actually the square of the average of the square root of the pressure, which we will refer as the average pressure. Using this average pressure will be useful to compare to simulations as well as theoretical estimates provided by Lindl.[51] The average shock breakout time is about 450 ps for all the experiments. This corresponds to the average pressure of 37 Mbars (where 1 Mbar is equal to 10^{12} dynes/cm^3). The complete experimental range of shock breakout times corresponds to pressures from 30 to 46 Mbars. The average pressure for the simulations was higher than this. It ranges from 33 to 64 Mbars. The higher pressure agrees with the finding that the simulation output showed earlier shock breakout times.

We can also compare this to theoretical estimates. From Lindl,

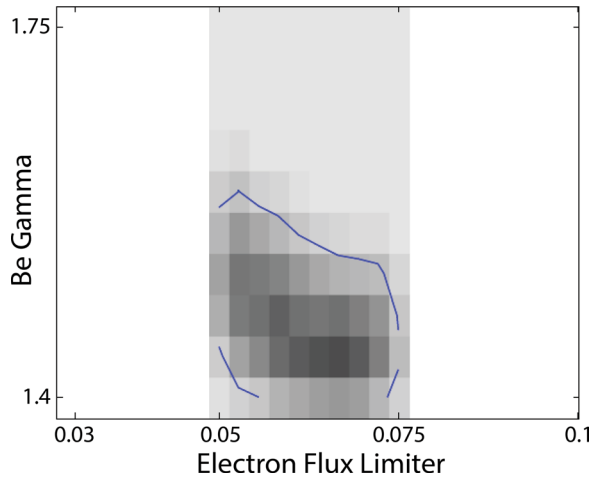

FIG. 12. Density plot of the posterior distribution for electron flux limiter and Be γ. This shows a preference of rate lower values of γ, consisted with the Be not being fully ionized.

$$P_{abl} \sim 8.0 * I_{14}^{2/3} \lambda_{\mu}^{-2/3} \text{Mbars}, \tag{3}$$

where $I_{14}^{2/3}$ is the laser irradiance in units of $10^{14}\,\text{W cm}^{-2}$. This equation was developed for plastic. For a laser irradiance of about $7 \times 10^{14}\,\text{W cm}^{-2}$ and $0.351\,\mu$m wavelength laser light, Eq. (3) estimates an ablation pressure of 59 Mbars. This is higher than the experiment, but within a factor of 2.

The study reported above was part of a multifaceted effort to employ statistical analysis and experiments with the purpose of improving the simulated results. The specific results presented above provided data to test all subsequent modeling of the earliest phases of the radiative shock experiments and provided a mean and probability distribution for the value of Be γ to use in a polytropic model of Be in this regime. Both these results proved useful as the model improved. Ultimately, to improve the agreement of the CRASH model and the data, relative to that shown in Figure 1, the largest single factor was to implement a laser-energy-deposition package within CRASH,[52,53] employing a 3D calculation of ray trajectories and energy deposition.

V. CONCLUSIONS

We have performed several shock breakout experiments to characterize the initial state of radiative shock experiments. Twelve experiments were performed and three instruments were used to infer the shock breakout time (2 VISARS and SOP). The average shock breakout time was 457 ps for the 10 experiments that used a nominal $20\,\mu$m Be disk. Two experiments were performed using a $10\,\mu$m Be disk and the average shock velocity in the Be was $44\,\mu\text{m ns}^{-1}$, which corresponds to an average pressure of 37 Mbars.

104 2D Hyades simulations were performed with various values of Be polytropic γ, electron flux limiter, Be thickness, laser energy, and polyimide tube wall opacity. The shock breakout time (defined as the time the shock reaches the rear of the Be disk for that particular simulation) was obtained from each simulation. The effects of varying each individual parameter was evaluated and Be γ was shown to have the negative correlation to shock breakout time with values of 1.4 to 1.55 comparable to the average experimental shock breakout time.

Electron flux limiter also has a negative correlation, but not as strongly as Be γ. This could be due to the large range of γ that was sampled. The majority of the shock breakout times from the simulation results were shorter than the experimental shock breakout time. Using a smaller value for the electron flux limiter would increase the shock breakout time for the simulation output. Values used when modeling similar experiments are 0.05 and 0.06. Be disk thickness has a positive correlation while laser energy and polyimide wall opacity have no correlation to the shock breakout time.

ACKNOWLEDGMENTS

The authors would like to acknowledge the support of Heather Wilkens and General Atomics in target characterization and development of stepped Be targets. These targets were fabricated by the Michigan Target Fabrication team with the assistance of Robb Gillespie. These experiments were performed at The Laboratory for Laser Energetics (LLE) with the support of many scientists and technicians. Valuable information for this paper was provided by Steve Stagnitto of LLE. Also, we thank Hye-Sook Park and Wolf Seka for meaningful conversations. This work was supported by the Predictive Sciences Academic Alliances Program in NNSA-ASC via Grant No. DEFC52-08NA28616, by the NNSA-DS and SC-OFES Joint Program in High-Energy-Density Laboratory Plasmas, Grant No. DE-FG52-09NA29548, and by the National Laser User Facility Program, Grant No. DE-NA0000850.

[1]N. Calvet and E. Gullbring, "The structure and emission of the accretion shock in T Tauri stars," Astrophys. J. **509**, 802–818 (1998).
[2]S. Lamzin, "X-ray emission from T Tauri stars attributable to an accretion shock wave," Astron. Lett. **25**, 430–436 (1999).
[3]J. Blondin, E. Wright, K. Borkowski, and S. Reynolds, "Transition to the radiative phase in supernova remnants," Astrophys. J. **500**, 342–354 (1998).
[4]L. Ensman and A. Burrows, "Shock breakout in SN-1987A," Astrophys. J. **393**, 742–755 (1992).
[5]C. Fransson, P. Lundqvist, and R. Chevalier, "Circumstellar interaction in SN 1993J," Astrophys. J. **461**, 993–1008 (1996).
[6]T. Nymark, C. Fransson, and C. Kozma, "X-ray emission from radiative shocks in type II supernovae," Astron. Astrophys. **449**, 171–192 (2006).
[7]R. Drake, "Radiative shocks in astrophysics and the laboratory," Astrophys. Space Sci. **298**, 49–59 (2005); in 5th International Conference on High Energy Density Laboratory Astrophysics, Tucson, AZ, 10–13 March 2004.
[8]C. Michaut, E. Falize, C. Cavet, S. Bouquet, M. Koenig, T. Vinci, A. Reighard, and R. P. Drake, "Classification of and recent research involving radiative shocks," Astrophys. Space Sci. **322**, 77 (2009).
[9]S. Bouquet, R. Teyssier, and J. Chieze, "Analytical study and structure of a stationary radiative shock," Astrophys. J., Suppl. Ser. **127**, 245 (2000).
[10]J. Bozier, G. Thiell, J. Lebreton, S. Azra, M. Decroisette, and D. Schirmann, "Experimental-observation of a radiative wave generated in xenon by a laser-driven supercritical shock," Phys. Rev. Lett. **57**, 1304–1307 (1986).
[11]P. Keiter, R. Drake, T. Perry, H. Robey, B. Remington, C. Iglesias, R. Wallace, and J. Knauer, "Observation of a hydrodynamically-driven, radiative-precursor shock," Phys. Rev. Lett. **89**, 165003 (2002).
[12]X. Fleury, S. Bouquet, C. Stehle, M. Koenig, D. Batani, A. Benuzzi-Mounaix, J. Chieze, N. Grandjouan, J. Grenier, T. Hall, E. Henry, J. Lafon, S. Leygnac, V. Malka, B. Marchet, H. Merdji, C. Michaut, and

F. Thais, "A laser experiment for studying radiative shocks in astrophysics," Laser Part. Beams **20**, 263–268 (2002); in Conference on Matter in Super-Intense Laser Fields: Short Pulse Superstrong Laser-Plasma Interactions, St Feliu de Guixols, Spain, 29 September-04 October 2001.
[13]A. Reighard, R. P. Drake, K. Danneberg, D. J. Kremer, T. Perry, B. Remington, R. Wallace, D. Ryutov, J. Greenough, J. Knauer, T. Boehly, S. Bouquet, A. Calder, R. Rosner, B. Fryxell, D. Arnett, M. Koenig, and N. Grandjouan, "Collapsing radiative shocks in xenon gas on the Omega laser," in *Proceedings of Inertial Fusion Science and Applications 2003* (Monterey CA, 2004), pp. 950–953.
[14]S. Bouquet, C. Stehle, M. Koenig, J. Chieze, A. Benuzzi-Mounaix, D. Batani, S. Leygnac, X. Fleury, H. Merdji, C. Michaut, F. Thais, N. Grandjouan, T. Hall, E. Henry, V. Malka, and J. Lafon, "Observation of laser driven supercritical radiative shock precursors," Phys. Rev. Lett. **92**, 225001 (2004).
[15]M. Koenig, T. Vinci, A. Benuzzi-Mounaix, S. Lepape, N. Ozaki, S. Bouquet, L. Boireau, S. Leygnac, C. Michaut, C. Stehle, J. Chieze, D. Batani, T. Hall, K. Tanaka, and M. Yoshida, "Radiative shock experiments at LULI," Astrophys. Space Sci. **298**, 69–74 (2005), in 5th International Conference on High Energy Density Laboratory Astrophysics, Tucson, AZ, 10–13 March 2004.
[16]M. Koenig, T. Vinci, A. Benuzzi-Mounaix, N. Ozaki, A. Ravasio, M. le Glohaec, L. Boireau, C. Michaut, S. Bouquet, S. Atzeni, A. Schiavi, O. Peyrusse, and D. Batani, "Radiative shocks: An opportunity to study laboratory astrophysics," Phys. Plasmas **13**, 056504 (2006); in 47th Annual Meeting of the Division of Plasma Physics of the American-Physical-Society, Denver, CO, 24–28 October 2005.
[17]F. W. Doss, R. P. Drake, and C. C. Kuranz, "Repeatability in radiative shock tube experiments," High Energy Density Phys. **6**, 157–161 (2010); in 2nd International Conference on High Energy Density Physics, Austin, TX, 19–22 May 2009.
[18]R. P. Drake, F. W. Doss, R. G. McClarren, M. L. Adams, N. Amato, D. Bingham, C. C. Chou, C. DiStefano, K. Fidkowski, B. Fryxell, T. I. Gombosi, M. J. Grosskopf, J. P. Holloway, B. van der Holst, C. M. Huntington, S. Karni, C. M. Krauland, C. C. Kuranz, E. Larsen, B. van Leer, B. Mallick, D. Marion, W. Martin, J. E. Morel, E. S. Myra, V. Nair, K. G. Powell, L. Rauchwerger, P. Roe, E. Rutter, I. V. Sokolov, Q. Stout, B. R. Torralva, G. Toth, K. Thornton, and A. J. Visco, "Radiative effects in radiative shocks in shock tubes," High Energy Density Phys. **7**, 130–140 (2011).
[19]J. Grun, J. Stamper, C. Manka, J. Resnick, R. Burris, J. Crawford, and B. Ripin, "Instability of Taylor-Sedov blast waves propagating through a uniform gas," Phys. Rev. Lett. **66**, 2738–2741 (1991).
[20]M. Edwards, A. MacKinnon, J. Zweiback, K. Shigemori, D. Ryutov, A. Rubenchik, K. Keilty, E. Liang, B. Remington, and T. Ditmire, "Investigation of ultrafast laser-driven radiative blast waves," Phys. Rev. Lett. **87**, 085004 (2001).
[21]J. F. Hansen, M. J. Edwards, D. H. Froula, A. D. Edens, G. Gregori, and T. Ditmire, "Laboratory observation of secondary shock formation ahead of a strongly radiative blast wave," Astrophys. Space Sci. **307**, 219–225 (2007); in 6th International Conference on High Energy Density Laboratory Astrophysics, Rice University, Houston, TX, 11–14 March 2006.
[22]A. S. Moore, E. T. Gumbrell, J. Lazarus, M. Hohenberger, J. S. Robinson, R. A. Smith, T. J. A. Plant, D. R. Symes, and M. Dunne, "Full-trajectory diagnosis of laser-driven radiative blast waves in search of thermal plasma instabilities," Phys. Rev. Lett. **100**, 055001 (2008).
[23]R. Peterson, D. Peterson, R. Watt, G. Idzorek, T. Tierney, and M. Lopez, "Blast wave radiation source measurement experiments on the Z Z-pinch facility," Phys. Plasmas **13**, 056901 (2006); in 47th Annual Meeting of the Division of Plasma Physics of the American-Physical-Society, Denver, CO, 24–28 October 2005.
[24]M. Hohenberger, D. R. Symes, J. Lazarus, H. W. Doyle, R. E. Carley, A. S. Moore, E. T. Gumbrell, M. M. Notley, R. J. Clarke, M. Dunne, and R. A. Smith, "Observation of a velocity domain cooling instability in a radiative shock," Phys. Rev. Lett. **105**, 205003 (2010).
[25]A. Reighard, R. Drake, K. Dannenberg, J. Knauer, and L. B. S. Bouquet, "Observation of collapsing radiative shock in laboratory experiments," Phys. Plasmas **13**, 082901 (2006).
[26]F. Doss, R. Drake, H. Robey, and C. Kuranz, "Wall shock in high-energy-density shock tube experiments," Phys. Plasmas **16**, 112705 (2009).
[27]F. Doss, R. Drake, and C. Kuranz, "Statistical inference in the presence of an inclination effet in laboratory radiative shock experiments," Astrophys. Space Sci. **336**, 219–224 (2010).
[28]C. C. Kuranz, R. P. Drake, C. M. Huntington, C. M. Krauland, C. A. Di Stefano, M. Trantham, M. J. Grosskopf, S. R. Klein, and D. C. Marion, "Early-time evolution of a radiative shock," High Energy Density Phys. **9**(2), 315–318 (2013).
[29]T. Boehly, D. Brown, R. Craxton, R. Keck, J. Knauer, J. Kelly, T. Kessler, S. Kumpman, S. Loucks, S. Letzring, F. Marshall, R. McCrory, S. Morse, W. Seka, J. Soures, and C. Verdon, "Initial performance results of the OMEGA laser system," Opt. Commun. **133**, 495–506 (1997).
[30]B. van der Holst, G. Toth, I. Sokolov, K. G. Powell, J. P. Holloway, E. Myra, Q. Stout, M. Adams, J. E. Morel, and R. P. Drake, "A block-adaptive-mesh code for radiative shock hydrodynamics: Implementation and verification," Astrophys. J. Suppl. Ser. **194**, 23 (2011).
[31]B. van der Holst, G. Toth, I. Sokolov, L. Daldorff, K. Powell, and R. Drake, "Simulating radiative shocks in nozzle shock tubes," High Energy Density Phys. **9**(1), 8–16 (2013).
[32]J. Larsen and S. Lane, "HYADES: A plasma hydrodynamics code for dense plasma studies," J. Quant. Spectrosc. Radiat. Transf. **51**, 179–186 (1994).
[33]D. E. Fratanduono, T. R. Boehly, P. M. Celliers, M. A. Barrios, J. H. Eggert, R. F. Smith, D. G. Hicks, G. W. Collins, and D. D. Meyerhofer, "The direct measurement of ablation pressure driven by 351-nm laser radiation," J. Appl. Phys. **110**, 073110 (2011).
[34]D. E. Fratanduono, J. H. Eggert, T. R. Boehly, M. A. Barrios, D. D. Meyerhofer, B. J. Jensen, and G. W. Collins, "Index of refraction of shock-released materials," J. Appl. Phys. **110**, 083509 (2011).
[35]C. Kuranz, R. Drake, K. Dannenberg, P. Susalla, D. Kremer, T. Boehly, and J. Knauer, "Preheat issues in hydrodynamic Hedla experiments," Astrophys. Space Sci. **298**, 267–271 (2005); in 5th International Conference on High Energy Density Laboratory Astrophysics, Tucson, AZ, 10–13 March 2004.
[36]D. K. Bradley, S. T. Prisbrey, R. H. Page, D. G. Braun, M. J. Edwards, R. Hibbard, K. A. Moreno, M. P. Mauldin, and A. Nikroo, "Measurements of preheat and shock melting in Be ablators during the first few nanoseconds of a National Ignition Facility ignition drive using the Omega laser," Phys. Plasmas **16**, 042703 (2009).
[37]M. A. Barrios, D. G. Hicks, T. R. Boehly, D. E. Fratanduono, J. H. Eggert, P. M. Celliers, G. W. Collins, and D. D. Meyerhofer, "High-precision measurements of the equation of state of hydrocarbons at 1-10 Mbar using laser-driven shock waves," Phys. Plasmas **17**, 056307 (2010); in 51st Annual Meeting of the Division-of-Plasma-Physics of the American-Physics-Society, Atlanta, GA, 02–06 November 2009.
[38]T. R. Boehly, V. N. Goncharov, W. Seka, M. A. Barrios, P. M. Celliers, D. G. Hicks, G. W. Collins, S. X. Hu, J. A. Marozas, and D. D. Meyerhofer, "Velocity and timing of multiple spherically converging shock waves in liquid deuterium," Phys. Rev. Lett. **106**, 195005 (2011).
[39]J. H. Eggert, D. G. Hicks, P. M. Celliers, D. K. Bradley, R. S. McWilliams, R. Jeanloz, J. E. Miller, T. R. Boehly, and G. W. Collins, "Melting temperature of diamond at ultrahigh pressure," Nat. Phys. **6**, 40–43 (2010).
[40]C. C. Kuranz, R. P. Drake, M. J. Grosskopf, A. Budde, C. Krauland, D. C. Marion, A. Visco, J. Ditmar, H. F. Robey, B. A. Remington, A. R. Miles, A. Cooper, C. Sorce, T. Plewa, N. C. Hearn, K. Killibrew, J. P. Knauer, and D. Arnett, "3D blast-wave-driven Rayleigh-Taylor instability and effects of long-wavelength modes," Phys. Plasmas **16**, 056310 (2009).
[41]L. Barker and R. Hollenback, "Laser interferometer for measuring high velocities of any reflecting surface," J. Appl. Phys. **43**, 4669 (1972).
[42]J. E. Miller, T. R. Boehly, A. Melchior, D. D. Meyerhofer, P. M. Celliers, J. H. Eggert, D. G. Hicks, C. M. Sorce, J. A. Oertel, and P. M. Emmel, "Streaked optical pyrometer system for laser-driven shock-wave experiments on OMEGA," Rev. Sci. Instrum. **78**, 034903 (2007).
[43]T. Boehly, personal communication (2004).
[44]R. Malone, R. McCrory, and R. Morse, "Indications of strongly flux-limited electron thermal conduction in laser-target experiments," Phys. Rev. Lett. **34**, 721–724 (1975).
[45]S. X. Hu, V. A. Smalyuk, V. N. Goncharov, S. Skupsky, T. C. Sangster, D. D. Meyerhofer, and D. Shvarts, "Validation of thermal-transport modeling with direct-drive, planar-foil acceleration experiments on OMEGA," Phys. Rev. Lett. **101**, 055002 (2008).
[46]R. P. Drake, *High-Energy-Density Physics: Fundamentals, Inertial Fusion, and Experimental Astrophysics* (Springer-Verlag, Berlin, 2006).
[47]A. Gelman and J. Hill, *Data Analysis Using Regression and Multilevel/Hierarchical Models* (Cambridge University Press, 2006).
[48]M. Kennedy and A. O'Hagan, "Bayesian calibration of computer models," J. R. Stat. Soc. Ser. B (Stat. Methodol.) **63**, 425–450 (2001).

[49]D. Higdon, M. Kennedy, J. Cavendish, J. Cafeo, and R. D. Ryne, "Combining field data and computer simulations for calibration and prediction," SIAM J. Sci. Comput. **26**, 448–466 (2004).
[50]C. Rasmussen and C. Williams, *Gaussian Processes for Machine Learning* (MIT Press, 2006), Vol. 1.
[51]J. Lindl, *Inertial Confinement Fusion* (Springer Verlag, New York, 1998).
[52]B. van der Holst, G. Toth, I. V. Sokolov, L. K. S. Daldorff, K. G. Powell, and R. P. Drake, "Simulating radiative shocks in nozzle shock tubes," High Energy Density Phys. **8**, 161–169 (2012).
[53]B. van der Holst, G. Tóth, I. Sokolov, B. Torralva, K. Powell, R. Drake, M. Klapisch, M. Busquet, B. Fryxell, and E. Myra, "Simulating radiative shocks with the crash laser package," High Energy Density Phys. **9**, 8–16 (2013).